

Robust multiple criteria decision making applied to optimization of AISI H13 hardened steel turning with PCBN wiper tool

Luiz Célio Souza Rocha¹ · Anderson Paulo de Paiva¹ · Paulo Rotela Junior² · Pedro Paulo Balestrassi¹ · Paulo Henrique da Silva Campos¹

Received: 25 June 2016 / Accepted: 25 July 2016 / Published online: 10 August 2016
© Springer-Verlag London 2016

Abstract Mathematically, each Pareto optimal point is an equally acceptable solution to a multiobjective optimization problem (MOP). However, the process of choosing a single preferred solution among all computed alternatives can be a difficult task because of a high cognitive effort required. Thus, the main objective of this work is to optimize the process of AISI H13 hardened steel turning with PCBN wiper tool using a robust multiple criteria decision making based on an entropic measure to choose the most preferred Pareto optimal point as the problem final solution. The responses of tool life (T), surface roughness parameter (Ra), and the ratio between material removal rate and cutting force (MRR/Fc) are modeled by using the response surface methodology (RSM), using as decision variables cutting speed (Vc), feed rate (f), and depth of cut (d). The normal boundary intersection (NBI) method along with the mixture design of experiments (MDE) are used to

optimize these responses simultaneously. The optimal turning process conditions obtained were judged satisfactory since that parameter values for cost, quality, and productivity are acceptable. Moreover, the study was able to demonstrate that the weights used in the multiobjective optimization process influence the prediction variance. From the variability point of view, the final solution obtained is the robust one, since it leads to a region of minimum variance, less variability, and greater reliability.

Keywords Hard turning · Wiper PCBN tool · Robust multiple criteria decision making · Normal boundary intersection · Entropic measure

1 Introduction

Precision hardened steel turning, i.e., turning process for materials which are hardened above 45 HRC [1–5], has been studied for more than 35 years [2] and, until the present moment, considerable attention has been given to its understanding [3–30]. This great number of studies was carried out on many materials and as the current state of knowledge in this field does not allow to generalize obtained results and to predict the behavior of other materials [5], the research on the machining of these materials is continued [11, 22].

When comparing with traditional grinding, the hard turning process shows some advantages such as the following: it reduces the manufacturing costs, reduces the setup time, it is flexible machining process, decreases production time, eliminates the cooling media, improves the surface integrity, and improves overall product quality [2–6, 8, 10, 21]. This process is widely used in the automotive, aerospace, gear, bearing, cam, forging, tools, and die industry [3, 5, 10, 21].

✉ Paulo Rotela Junior
paulo.rotela@gmail.com

Luiz Célio Souza Rocha
luizrochamg@hotmail.com

Anderson Paulo de Paiva
andersonppaiva@unifei.edu.br

Pedro Paulo Balestrassi
ppbalestrassi@gmail.com

Paulo Henrique da Silva Campos
paulohcampos@hotmail.com

¹ Institute of Production Engineering and Management - Federal University of Itajubá, Itajubá, MG, Brazil

² Department of Production Engineering, Federal University of Paraíba Cidade Universitária - Campus I, João Pessoa 58051-900, PB, Brazil

In finish hard turning, high hardness of workpieces, large cutting forces, and high temperatures at the cutting tool-workpiece interface impose extreme requirements for tool rigidity and tool wear resistance [21]. Due to this condition, PCBN has proved to be better for producing precise parts than coated micrograin carbides and ceramics [23]. PCBN is the second hardest material known to man after diamond [24, 25] with high hardness also at high temperatures. It has high thermal stability and high thermal conductivity [26–29]. The commercial PCBN tool material consists of cBN grains, surrounded by a matrix with TiCN, Al_2O_3 , and WC. Al is added to the material in order to react with the oxygen present in the material in the high-temperature, high-pressure treatment during manufacturing. It is also there to promote the sintering process [25]. The PCBN diffractogram is shown in Fig. 1.

About the contribution of the tool geometry for the improvement of hard turning process, some authors present the use of tools with wiper geometry [3, 4, 7, 10, 30]. Due to its three radii geometry [3], as shown in Fig. 2, it is possible to double the feed rate, increasing the productivity and also keeping the surface roughness as low as possible [3, 10, 30].

The potential benefits promoted by hard turning for surface quality and the increasing of productivity rate depend intrinsically on an optimal setup for the process parameters such as cutting speed (V_c), feed rate (f), and depth of cut (d). These parameters are directly responsible for many of machining predictable properties like tool wear, tool life, surface finishing, and amount of material removed [3, 10, 14, 30].

Analyzing manufacturing processes, of which the machining process is an example, it appears that the various possibly controlled parameters lead to multiobjective mathematical models in order to ensure its optimization.

When working with multiobjective optimization, in addition to the search for the point that characterizes the problem

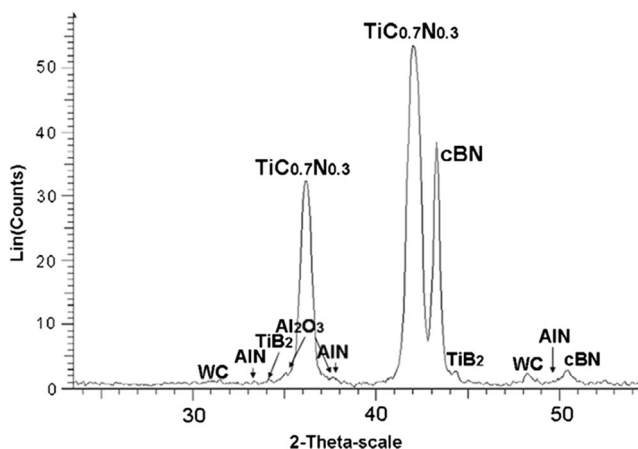


Fig. 1 X-ray diffraction (XRD) results from PCBN material [25]

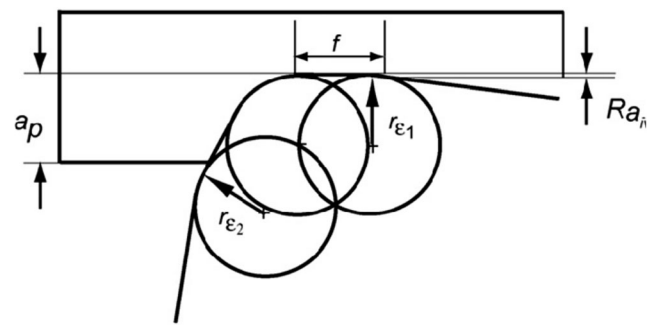


Fig. 2 Wiper insert design: r_{ϵ_1} and r_{ϵ_2} are the radii of wiper curvature [3]

final solution, how reliable is this solution appears as a central point. Therefore, the forecast variance is a major concern [31]. About this subject, the discussion of how the weighting in multiobjective optimization affects the forecast variance, given a certain experimental design, was not made, making it clear that theoretical contributions can be given to explore this topic.

Thus, the main objective of this work is to optimize the process of AISI H13 hardened steel turning with PCBN wiper tool using a robust multiple criteria decision making based on an entropic measure to choose the most preferred Pareto optimal point as the problem final solution. The responses of tool life (T), surface roughness parameter (Ra), and the ratio between material removal rate and cutting force (MRR/F_c) are modeled by using the response surface methodology (RSM), and the normal boundary intersection (NBI) method along with the mixture design of experiments (MDE) are used to optimize these responses simultaneously. The decision variables are cutting speed (V_c), feed rate (f), and depth of cut (d).

2 Design of experiments

According to Montgomery [32], an experiment can be defined as a series of tests in which purposeful changes are made to the input variables of a process, aiming thereby to observe how such changes affect the responses. Design of experiments (DOE) is then defined as the process of planning experiments so that appropriate data is collected and then analyzed by statistical methods, leading to valid and objective conclusions.

Regarding the experimental projects, the most widely used techniques include the RSM and MDE.

RSM is a collection of mathematical and statistical tools used to model and analyze problems in which responses of interest are influenced by several variables. The objective of RSM is to optimize these responses [32, 33].

For most industrial processes, the relationships between responses and independent variables are unknown, so RSM seeks to find a suitable approximation to represent the responses of interest as a function of these variables. To describe such relationships, researchers generally use polynomial functions. Thus, if a response is well modeled by a quadratic function, the approximate ratio can be represented by the following second-order model:

$$\hat{y} = \hat{\beta}_0 + \sum_{i=1}^k \beta_i x_i + \sum_{i=1}^k \beta_{ii} x_i^2 + \sum_{i < j} \beta_{ij} x_i x_j + \varepsilon \quad (1)$$

where $y(x)$ is the response of interest, x_i is an independent variable, β_0 is the intercept coefficient to be estimated, β_i is the linear coefficient to be estimated, β_{ii} is the squared coefficient to be estimated, k is the number of independent variables, and ε is the experimental error.

While it is unlikely for a polynomial model to behave as a proper approach for the entire experimental space covered by the independent variables, such models have been shown to be effective for a specific region [32, 33].

The estimation of coefficients, defined by Eq. 1, is typically made using the ordinary least squares (OLS) method. The OLS method is based on choosing values for β_i , such that the sum of squared errors is minimized. The OLS function can be written as follows [32, 33]:

$$L = \sum_{i=1}^k \varepsilon_i^2 = \sum_{i=1}^k \left(y_i - \beta_0 - \sum_{i=1}^k \beta_i x_i \right)^2 \quad (2)$$

where y_i is the response of interest, x_i is an independent variable, β_i is the coefficient to be estimated, k is the number of independent variable, and ε_i is the experimental error.

The response of interest may be written in matrix notation as

$$\mathbf{y} = \mathbf{X}\boldsymbol{\beta} + \boldsymbol{\varepsilon} \quad (3)$$

where

$$\mathbf{y} = \begin{bmatrix} y_1 \\ y_2 \\ \vdots \\ y_n \end{bmatrix}, \mathbf{X} = \begin{bmatrix} 1 & x_{11} & x_{12} & \cdots & x_{1k} \\ 1 & x_{21} & x_{22} & \cdots & x_{2k} \\ \vdots & \vdots & \vdots & \ddots & \vdots \\ 1 & x_{n1} & x_{n2} & \cdots & x_{nk} \end{bmatrix}, \boldsymbol{\beta} = \begin{bmatrix} \beta_0 \\ \beta_1 \\ \vdots \\ \beta_k \end{bmatrix}, \boldsymbol{\varepsilon} = \begin{bmatrix} \varepsilon_1 \\ \varepsilon_2 \\ \vdots \\ \varepsilon_n \end{bmatrix} \quad (4)$$

Thus, L can be expressed as

$$\begin{aligned} L &= \mathbf{y}^T \mathbf{y} - \boldsymbol{\beta}^T \mathbf{X}^T \mathbf{y} - \mathbf{y}^T \mathbf{X} \boldsymbol{\beta} + \boldsymbol{\beta}^T \mathbf{X}^T \mathbf{X} \boldsymbol{\beta} \\ &= \mathbf{y}^T \mathbf{y} - 2\boldsymbol{\beta}^T \mathbf{X}^T \mathbf{y} + \boldsymbol{\beta}^T \mathbf{X}^T \mathbf{X} \boldsymbol{\beta} \end{aligned} \quad (5)$$

Since $\boldsymbol{\beta}^T \mathbf{X}^T \mathbf{y}$ is a 1×1 matrix, or a scalar, and its transpose $(\boldsymbol{\beta}^T \mathbf{X}^T \mathbf{y})^T = \mathbf{y}^T \mathbf{X} \boldsymbol{\beta}$ is the same scalar, the least squares estimators must satisfy

$$\frac{\partial L}{\partial \boldsymbol{\beta}} = -2\mathbf{X}^T \mathbf{y} + 2\mathbf{X}^T \mathbf{X} \hat{\boldsymbol{\beta}} = 0 \quad (6)$$

which simplifies to

$$\mathbf{X}^T \mathbf{X} \hat{\boldsymbol{\beta}} = \mathbf{X}^T \mathbf{y} \quad (7)$$

Equation 7 is the set of least squares normal equations in matrix form. By multiplying both sides of Eq. 7 by the inverse of $\mathbf{X}^T \mathbf{X}$, we have

$$\hat{\boldsymbol{\beta}} = (\mathbf{X}^T \mathbf{X})^{-1} \mathbf{X}^T \mathbf{y} \quad (8)$$

As the least squares estimator $\hat{\boldsymbol{\beta}}$ is a linear combination of the observations, it is normally distributed with mean vector $\boldsymbol{\beta}$ and covariance matrix $\sigma^2 (\mathbf{X}^T \mathbf{X})^{-1}$. Then, the statistic

$$\frac{\hat{\beta}_j - \beta_j}{\sqrt{\sigma^2 C_{jj}}}, \quad j = 0, 1, \dots, k \quad (9)$$

is distributed as t with $n-p$ degrees of freedom, where C_{jj} is the jj th element of the matrix $(\mathbf{X}^T \mathbf{X})^{-1}$, and σ^2 is the estimate of the error variance, obtained from equation:

$$\hat{\sigma}^2 = \frac{SS_E}{n-p} \quad (10)$$

where SS_E is the residual (or error) sum of squares and is given by

$$SS_E = \mathbf{y}^T \mathbf{y} - \boldsymbol{\beta}^T \mathbf{X}^T \mathbf{y} \quad (11)$$

Therefore, a confidence interval of $100(1-\alpha)\%$ for the regression coefficient $\beta_j, j=0, 1, \dots, k$, is given by

$$\hat{\beta}_j - t_{\alpha/2, n-p} \sqrt{\hat{\sigma}^2 C_{jj}} \leq \beta_j \leq \hat{\beta}_j + t_{\alpha/2, n-p} \sqrt{\hat{\sigma}^2 C_{jj}} \quad (12)$$

Note that this confidence interval can be written as a function of the regression coefficient standard error $se(\hat{\beta}_j)$:

$$\hat{\beta}_j - t_{\alpha/2, n-p} se(\hat{\beta}_j) \leq \beta_j \leq \hat{\beta}_j + t_{\alpha/2, n-p} se(\hat{\beta}_j) \quad (13)$$

because $se(\hat{\beta}_j) = \sqrt{\sigma^2 C_{jj}}$.

We may also obtain the mean response confidence interval at a particular point $\mathbf{X}_0^T = [1 \ x_{01} \ x_{02} \ \dots \ x_{0k}]$. The mean response at this point is given by $\mu_{y|\mathbf{X}_0} = \mathbf{X}_0^T \boldsymbol{\beta}$, and the estimated mean response at this point is given by $y^\wedge(\mathbf{X}_0) = \mathbf{X}_0^T \boldsymbol{\beta}^\wedge$. This estimator is an unbiased one, because $E[y^\wedge(\mathbf{X}_0)] = E(\mathbf{X}_0^T \boldsymbol{\beta}^\wedge) = \mathbf{X}_0^T \boldsymbol{\beta} = \mu_{y|\mathbf{X}_0}$ and the variance of $y^\wedge(\mathbf{X}_0)$ is

$$\text{Var}[y^\wedge(\mathbf{X}_0)] = \sigma^2 \mathbf{X}_0^T (\mathbf{X}^T \mathbf{X})^{-1} \mathbf{X}_0 \tag{14}$$

Therefore, a confidence interval of $100(1-\alpha)\%$ on the mean response at the point $\mathbf{X}_0^T = [1 \ x_{01} \ x_{02} \ \dots \ x_{0k}]$ is

$$y^\wedge(\mathbf{X}_0) - t_{\alpha/2, n-p} \sqrt{\sigma^2 \mathbf{X}_0^T (\mathbf{X}^T \mathbf{X})^{-1} \mathbf{X}_0} \leq \mu_{y|\mathbf{X}_0} \leq y^\wedge(\mathbf{X}_0) + t_{\alpha/2, n-p} \sqrt{\sigma^2 \mathbf{X}_0^T (\mathbf{X}^T \mathbf{X})^{-1} \mathbf{X}_0} \tag{15}$$

After constructing the model, the statistical significance of the same should be verified through analysis of variance (ANOVA). ANOVA, apart from revealing the significance of the model as a whole, permits one to check which of the model’s terms are significant and which may be neglected.

The fit is represented by the coefficient of multiple determination (R^2), which represents the percentage of the observed data in the response that can be explained by the mathematical model. R^2 is defined as

$$R^2 = \frac{SS_R}{SS_T} = 1 - \frac{SS_E}{SS_T} \tag{16}$$

where SS_R is the regression sum of squares; SS_E is the residual (or error) sum of squares, as presented in Eq. 11; and SS_T is the total sum of squares.

The regression sum of squares (SS_R) may be presented as

$$SS_R = \boldsymbol{\beta}^T \mathbf{X}^T \mathbf{y} - \frac{\left(\sum_{i=1}^n y_i\right)^2}{n} \tag{17}$$

and, the total sum of squares (SS_T) is

$$SS_T = \mathbf{y}^T \mathbf{y} - \frac{\left(\sum_{i=1}^n y_i\right)^2}{n} \tag{18}$$

In using a more accurate parameter, an adjusted R^2 can be defined as

$$R_{adj}^2 = 1 - \frac{n-1}{n-p} (1-R^2) \tag{19}$$

where n is the number of experiments and p is the number of terms plus one (related to the intercept).

For the modeling of the response surface functions, the experimental arrangement most often used for data collection is the central composite design (CCD) [32]. CCD, for k factors, is a matrix formed by three distinct groups of experimental elements: a full factorial 2^k or fractional 2^{k-p} , where p is the desired fraction of the experiment; a set of central points (cp); and, in addition, a group of extreme levels called axial points, given by $2k$. The number of experiments required is given by the sum: 2^k or $(k-p) + cp + 2k$. In CCD, the axial points are within a distance α of the central points, being $\alpha = (2^k)^{1/4}$ [34].

In MDE, the factors are the ingredients of a mixture and their levels are not independent. Due to the existence of the constraint $\sum_{i=1}^n x_i = 1$, the mixture models have some differences from polynomials employed in RSM. For example, the special cubic form is [32, 35]

$$y = \sum_{i=1}^q \beta_i x_i + \sum_{i < j}^q \beta_{ij} x_i x_j + \sum_{i < j < k}^q \beta_{ijk} x_i x_j x_k \tag{20}$$

According to Cornell [35] and Anderson-Cook et al. [31], the different shape of the previous function makes it to be called Scheffé’s polynomials or canonical polynomials of mixtures.

The estimation of the coefficients is done in a similar way to that used in RSM, the same occurring for statistical tests as ANOVA.

The experimental arrangement most used in MDE is the simplex arrangement [35]. In this, the k input variables define points whose proportions are assumed to take into consideration $m + 1$ equally spaced values between 0 and 1, where m is the lattice degree of the arrangement. The total number of experiments (N) is given by

$$N = \frac{(k + m - 1)!}{m!(k - 1)!} \tag{21}$$

As in simplex arrangement, most experiments occur at the borders of the array few points of the internal part are tested. Due to this feature, it is important to add internal points to the arrangements, as the central points and the axial points.

3 Multiobjective optimization

The optimization problems involving industrial processes are often multiobjective, since they involve more than one

desirable feature. If there is no conflict between the objective functions, then a solution can be found where each objective function reaches its optimum. In this case, no special method is required [36].

However, often these goals are function of the same decision variable set and are conflicting [37]. To study the tradeoffs between these conflicting objectives and explore the options available, one must formulate a multiobjective optimization problem (MOP). A general formulation may be presented as

$$\text{Min}_{x \in \Omega} \Lambda = \{F_1(x), F_2(x), \dots, F_k(x)\} \tag{22}$$

where Λ is the vector of objective functions consisting of k criteria, F_i , which are mutually conflicting. The decision variables vector, x , must belong to the feasible set Ω which usually includes the problem constraints in inequalities or equalities form:

$$\Omega = \{x \in \mathbb{R}^n \mid g_r(x) \leq 0, r \in I, h_q(x) = 0, q \in J\} \tag{23}$$

where g_r and h_q are the inequality and equality constraint functions, respectively; I and J are the index sets containing as many elements as there are inequality and equality constraints, respectively.

The multiobjective optimization methods attempt to produce a set of tradeoff solutions called Pareto optimal solutions, of which the decision maker can choose one. A solution is called Pareto optimal if no objective can be improved without sacrificing the other. Methods that allow obtaining the full set of Pareto optimal solutions should have priority in use as they provide the decision-maker the ability to select the best solution among those considered efficient.

According to Shahraki and Noorossana [38], there are two approaches to solve problems with more than one objective function. The former is based on optimizing an objective considering other objectives as constraints. In this context, the considered most important objective function is prioritized, giving rise to the term prioritization. The latter is based on converting all objective functions in one, by reducing it to a scalar optimization problem; hence, the term scalarization. Scalarization is the conversion of the problem, by aggregation of the components of the objective functions, into a single or a family of single objective optimization problems with a real-valued objective function [36, 39]. Many methods can be used for this purpose, among which are the weighted sum method and the normal boundary intersection (NBI) approach.

3.1 Weighted sum method

The weighted sum method is one of the most used techniques for solving MOP. According to Zhang and Yang [40], this is

due to its relative simplicity and physical interpretation of the processes being analyzed.

This method is characterized as a sequence of problems in which the objective functions are converted into a scalar optimization problem by minimizing the objective convex combination of the different objectives, i.e., the global objective function is defined by a linear combination of the original objective function and their respective degrees of importance represented by the weights. In other words, n weights w_i are chosen, such that $w_i \geq 0, i = 1, \dots, n$ and $\sum_{i=1}^n w_i = 1$ and the following problem is solved:

$$\begin{aligned} \text{Min}_x \quad & \sum_{i=1}^n w_i f_i(x) = w^T F(x) \\ \text{s.t.} \quad & h_i(x) = 0, i = 1, 2, \dots, l \\ & g_j(x) \leq 0, j = 1, 2, \dots, m \end{aligned} \tag{24}$$

where $f_i(x)$ is the $n \geq 2$ objective functions to be optimized, $h_i(x)$ represents the l equality constraints, and $g_j(x)$ represents the m inequality constraints.

It follows immediately that the global minimizer x^* of the above problem is a Pareto optimal point for MOP. If this is not true, then there should be a feasible x in which one objective could be improved without sacrificing the others [41].

A common approach is to perform the minimization described in Eq. 24 repeatedly using an even dispersion of the weight w in order to generate many points in the Pareto optimal set. However, according to Das and Dennis [41], there are difficulties related to this practice: (1) if the Pareto frontier is nonconvex, there is no weight w for which the solution of the problem remains in the nonconvex area; (2) even with a convex Pareto frontier, a uniform distribution of w , does not produce a uniform distribution of points on the Pareto frontier. Thus, even if a uniform spread of weight vectors is used, the Pareto frontier will be neither equispaced nor evenly distributed.

According to Shin et al. [42], a multiobjective problem is convex if the feasible set Ω is convex and the functions are also convex. When at least one objective function is nonconvex, the multiobjective problem becomes nonconvex, generating a nonconvex and even not connected Pareto frontier. When working with nonconvex Pareto frontiers, points in the concave area cannot be reached by minimizing the objectives convex combination [41]. This instability is due to the fact that the weighted sum is not a Lipschitzian function of the weight w [43].

In RSM, one way to determine the convexity of a function is by characterizing the nature of the stationary point. The stationary point is the level of x_1, x_2, \dots, x_k , that optimize the predicted response. This point, if it exists, will be the set of x_1, x_2, \dots, x_k , for which the partial derivatives equal to zero. A general mathematical solution for the location of the stationary

point may be obtained. The second-order model may be expressed in matrix notation as follows [32, 33]:

$$\hat{y} = \hat{\beta}_0 + \mathbf{x}^T \mathbf{b} + \mathbf{x}^T \mathbf{B} \mathbf{x} \tag{25}$$

where

$$\mathbf{x} = \begin{bmatrix} x_1 \\ x_2 \\ \vdots \\ x_k \end{bmatrix}, \mathbf{b} = \begin{bmatrix} \hat{\beta}_1 \\ \hat{\beta}_2 \\ \vdots \\ \hat{\beta}_k \end{bmatrix}, \mathbf{B} = \begin{bmatrix} \hat{\beta}_{11} & \hat{\beta}_{12}/2 & \cdots & \hat{\beta}_{1k}/2 \\ \hat{\beta}_{21}/2 & \hat{\beta}_{22} & \cdots & \hat{\beta}_{2k}/2 \\ \vdots & \vdots & \ddots & \vdots \\ \hat{\beta}_{k1}/2 & \hat{\beta}_{k2}/2 & \cdots & \hat{\beta}_{kk} \end{bmatrix} \text{ for } \hat{\beta}_{ij} = \hat{\beta}_{ji} \tag{26}$$

The derivative of y^\wedge with respect to the elements of the vector \mathbf{x} equated to zero is

$$\frac{\partial y^\wedge}{\partial \mathbf{x}} = \mathbf{b} + 2\mathbf{B}\mathbf{x} = 0 \tag{27}$$

The stationary point is the solution to Eq. 26:

$$\mathbf{x}_s = -\frac{1}{2} \mathbf{B}^{-1} \mathbf{b} \tag{28}$$

And the predicted response at the stationary point is

$$\hat{y}_s = \hat{\beta}_0 + \frac{1}{2} \mathbf{x}_s^T \mathbf{b} \tag{29}$$

The nature of the stationary point is determined from the sign of the eigenvalues or characteristic roots of the matrix \mathbf{B} . The eigenvalues (λ_i) of the matrix \mathbf{B} are the solutions to the equation:

$$|\mathbf{B} - \lambda \mathbf{I}| = 0 \tag{30}$$

If the λ_i are all negative, then the function is concave and \mathbf{x}_s is a point of maximum; if the λ_i are all positive, then the function is convex and \mathbf{x}_s is a point of minimum. However, if the λ_i have different signs, the function is neither concave nor convex and \mathbf{x}_s is a saddle point.

3.2 Normal boundary intersection

A standard method for generating the Pareto set in MOP is the weighted sum method. However, according to Das and Dennis [41], this method can only obtain points from all parts of the Pareto frontier when it is convex. Furthermore, an evenly distributed set of weights fails to produce an even distribution of points from all parts of the Pareto frontier, even for convex ones.

In order to overcome the drawbacks of the weighted sum method, Das and Dennis [44] proposed the NBI method, showing that the Pareto surface is evenly distributed independent of the relative scales and convexity of the objective functions.

The establishment of the payoff matrix Φ is the first step of this method. In matrix notation, Φ can be written as follows [43, 45]:

$$\Phi = \begin{bmatrix} f_1^*(x_1^*) & \cdots & f_1(x_i^*) & \cdots & f_1(x_m^*) \\ \vdots & \ddots & \vdots & \ddots & \vdots \\ f_i(x_1^*) & \cdots & f_i^*(x_i^*) & \cdots & f_i(x_m^*) \\ \vdots & \ddots & \vdots & \ddots & \vdots \\ f_m(x_1^*) & \cdots & f_m(x_i^*) & \cdots & f_m^*(x_m^*) \end{bmatrix} \tag{31}$$

Each row of Φ consists of minimum and maximum values of the i th objective function $f_i(x)$. These values can be used to normalize the objective functions, generating the normalized payoff matrix Φ . This procedure is used when the objective functions are written in different units and can be expressed as follows [43]:

$$f(x) = \frac{f_i(x) - f_i^U}{f_i^N - f_i^U}, \quad i = 1, \dots, m \tag{32}$$

where $f_i(x)$ is the individual values of the objectives, f_i^U is the Utopia point, and f_i^N is the Nadir point.

The Utopia point is a specific point, generally outside of the feasible region, that corresponds to all objectives simultaneously being at their best possible values and may be written as $f^U = [f_1^*(x_1^*), \dots, f_i^*(x_i^*), \dots, f_m^*(x_m^*)]^T$. Nadir point is a point in the design space where all objectives are simultaneously at their worst values and may be written as $f^N = [f_1^N, \dots, f_i^N, \dots, f_m^N]^T$.

The convex hull of individual minimum (CHIM) is comprised by the convex combinations of each row of Φ . The anchor points which correspond to the solution of single optimization problem $f_i^*(x_i^*)$ are connected by the Utopia line [45]. If Φw_i is a point in the CHIM, e is a column vector of ones and D is the distance between the Utopia line and the Pareto frontier, the intersection point between the normal with $\Phi w - D\Phi e$ representing the set of points on that normal and the boundary of the feasible region corresponds to the maximization of D . Thus, the NBI method is used to solve the MOP, using the following equation [44]:

$$\begin{aligned} & \text{Max } D \\ & (x, D) \\ & \text{s.t. : } \Phi w - D\Phi e = F(\mathbf{x}) \\ & \mathbf{x} \in \Omega \end{aligned} \tag{33}$$

where w is the convex weighting, D is the distance between the Utopia line and the Pareto frontier, $F(\mathbf{x})$ is the vector containing the individual values of the normalized objectives

in each run, e is a column vector of ones, and Φ is the normalized payoff matrix.

This problem can be solved iteratively for different values of w , creating a Pareto frontier uniformly distributed [43, 46]. A common choice for w is $w_n = 1 - \sum_{i=1}^{n-1} w_i$ [44, 47].

4 Weighting methods applied to multiobjective optimization

When trying to solve a MOP, we are interested in finding efficient solutions. Efficiency is a concept equivalent to the Pareto optimality, noninferiority, and nondominance. However, usually, there are many efficient solutions (an infinite number), forming the efficient set or Pareto optimal set [36]. According to Mela et al. [48], the process of generating Pareto optimal alternatives is called multiobjective optimization.

Mathematically, each Pareto optimal point is an equally acceptable solution to a MOP [36], generally being desirable to obtain a point as the final solution. However, due to the multidisciplinary nature of the problems related to machining processes which are closely related to several multiple criteria noncommensurable, to determine which solution is the best choice to be implemented can be a difficult task. According to Mela et al. [48], the process of choosing a single preferred solution among all computed alternatives is called multiple criteria decision making.

Since it is difficult to know the importance degree to be assigned to each objective [49], the weight definition for each function is eventually made subjectively influenced by the analyst’s preferences. By assigning different weights to the representative objective functions of the processes characteristics that we want to optimize, we consider the relative importance of each parameter within the analyzed process. This means that weights should be assigned to functions to indicate their relative importance in order to identify what really matters during the optimization process, thus electing priorities [50].

The priority assigned to the criteria has vital role in achieving results and should be applied with caution, since the end result can vary significantly depending on the importance attached to each objective [51–53]. This can be a problem, because decision makers often are not sure about the exact weights of objective functions either utility functions to be used [51]. Indeed, to elicit direct preference information from the analyst can be counterproductive in real-world decision-making because of a high cognitive effort required [54].

According to Taboada et al. [51], the Pareto set includes all rational choices, among which the decision maker must select the final solution, comparing the

several objectives against each other. The search is, therefore, not by an optimal solution but a set of solutions that are optimal in the widest sense, i.e., they are Pareto optimal. There are several techniques to search on solution space a set of Pareto optimal solutions. Probably, the main drawback of these methods is that the decision maker has many solutions from which to choose. Thus, it is necessary to bridge the gap between the unique solutions and Pareto optimal sets [51].

The weighting issue has been discussed in literature for at least 40 years. Zeleny [55, 56], when solving a linear multiobjective optimization problem, aimed to answer the following questions: Which of generated nondominated extreme solutions is the most preferred? Can the set of nondominated solutions be reduced so it would consist of few enough points so that the final decision could be made? To answer such questions, the author uses what he called “traditional entropy measure” as a parameter to gauge the functions importance and to define the weights to be used in solving the problem.

Recently, Rocha et al. [57, 58] used Shannon entropy index [59] associated with an error measure, the global percentage error (GPE), in order to determine the most preferred Pareto optimal point in a vertical turning MOP solved by NBI method. According to the authors, Shannon’s entropy can provide a more reliable assessment of the relative weights for the objectives in the absence of the decision maker’s preferences and, in association with an error measure, it minimized the error of the preferred Pareto optimal point related to the individual optimal responses. The weighting metric ξ , proposed by Rocha et al. [57, 58], is obtained using the equation

$$\begin{aligned} \text{Max } \xi &= \frac{\text{Entropy}}{\text{GPE}} \\ \text{s.t. : } \sum_{i=1}^n w_i &= 1 \\ 0 \leq w_i &\leq 1 \end{aligned} \tag{34}$$

where w_i is the weight assigned to the objectives to be optimized.

The *Entropy* in Eq. 34 is calculated as follows [59]:

$$\text{Entropy} = - \sum_{i=1}^m w_i \ln w_i \tag{35}$$

And the *GPE* in Eq. 34 is calculated as follows [60]:

$$\text{GPE} = \sum_{i=1}^m \left| \frac{y_i^*}{T_i} - 1 \right| \tag{36}$$

where y_i^* is the value of the Pareto-optimal responses, T_i is the defined target, and m is the number of objectives.

5 Experimental design and robust multiple criteria decision making

To carry out this work, dry turning tests of the AISI H13 steel, with chemical composition of 0.40 % C, 0.35 % Mn, 1.0 % Si, 5.25 % Cr, 1.00 % V, and 1.50 % Mo, were performed using a CNC lathe with maximum rotational speed of 4500 rpm and power of 18 kW. The workpieces used in the turning process were made with dimensions of $\varnothing 50 \text{ mm} \times 100 \text{ mm}$. All of them were previously quenched in a vacuum atmosphere at 1000–1040 °C and tempered. After this heat treatment, an average hardness of $54 \pm 1 \text{ HRC}$ was obtained. Wiper PCBN (cBN + TiC) inserts, Ref. PCBN7025 (ISO code-CNGA 120408 S01030 AWG), were used to machining of AISI H13 hardened steel. The tool holder used in the experiments presented a negative geometry with ISO code DCLNL 2020K12 and entering angle $\chi_r = 95^\circ$. Figure 3 represents the cutting tool and the turning process of AISI H13 hardened steel used in the experimental study.

The measurement of surface roughness parameter (Ra) on finish turning surfaces was made by a stylus instrument in accordance to ISO/DIS 4287/1E. In hard turning, the cutting tool is subjected to higher temperature and pressure near the nose, resulting in formation of flank and crater wear. The evaluation of the flank tool wear was made by a toolmaker's microscope with $30\times$ magnification and $1\text{-}\mu\text{m}$ resolution. The admissible flank wear ($VB = 0.30 \text{ mm}$) was established according ISO 3685 standard and measured at corner radius with scanning electron microscopy (SEM) after each run. Figure 4 shows the flank and crater wear of cutting tool.

The acquisition of the cutting force (F_c) was performed by a piezoelectric dynamometer. The values were continuously monitored and recorded throughout the test by using a charge amplifier with data acquisition capability. The material removal rate (MRR) is calculated as the volume of material removed divided by the time taken to remove it. By using the ratio MRR/F_c , a productivity parameter can be defined, in the same way of the specific cutting energy. However, in the case of the ratio MRR/F_c , the maximization is desirable.

Adopting this experimental condition, the workpieces were machined using the range of parameters as defined in Table 1. The decision variables have been analyzed in a coded way in order to reduce the variance. Only at the end of the analyses they have been converted to their uncoded values, by using

$$X_{\text{uncoded}} = \frac{Hi + Lo}{2} + X_{\text{coded}} \frac{Hi - Lo}{2} \quad (37)$$

where Hi is related to the value of level +1 and Lo is related to the value of level -1.

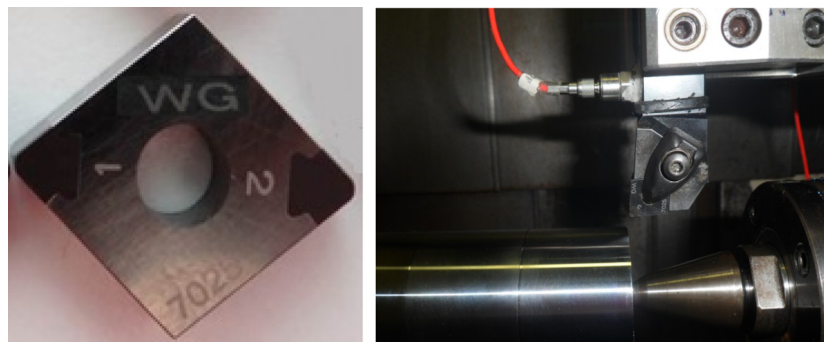
A sequential set of experimental runs was established using a CCD built according to a response surface design 2^3 , with 6 axial points and 5 center points, generating 19 experiments (Table 2).

In order to optimize T , Ra , and MRR/F_c at the same time, the multiple criteria decision making process described in Rocha et al. [58] has been used. It aims to build an evenly distributed Pareto frontier and to choose one preferred Pareto optimal point as the final solution of the problem. In this process, as the NBI method has been used, there exists no drawback related to weighted sum method. Furthermore, in order to verify the robustness of the final result obtained with the employed multiobjective optimization process, a metric of variance has been calculated. According to Zahran et al. [61], several measures of prediction performance exist for comparing experimental designs, being the scaled prediction variance (SPV) the most commonly considered. SPV is defined as $N \text{Var}[y^\wedge(\mathbf{X}_0)] / \sigma^2 = N \mathbf{X}_0^T (\mathbf{X}^T \mathbf{X})^{-1} \mathbf{X}_0$, where N is the total sample size. However, if direct comparisons between the expected variance of estimation is desired, the unscaled prediction variance (UPV) could be modeled directly by the variance of the estimated mean response divided by σ^2 : $\text{Var}[y^\wedge(\mathbf{X}_0)] / \sigma^2 = \mathbf{X}_0^T (\mathbf{X}^T \mathbf{X})^{-1} \mathbf{X}_0$. It is equivalent to the hat matrix [33].

The step-by-step procedure is described as follows:

- Step 1. DOE: It is the establishment of the experimental design and execution of experiments in random order.

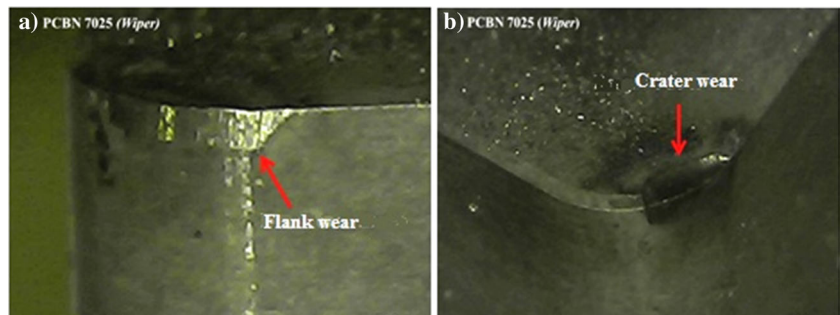
Fig. 3 Hard turning process with wiper PCBN tool. **a** Wiper PCBN 7025 tool. **b** Hard turning process



(a) Wiper PCBN 7025 tool

(b) Hard turning process

Fig. 4 SEM images of the flank and crater wear of cutting tool



- Step 2. Objective functions modeling: It is the equations definition using experimental data.
- Step 3. MOP formulation: The NBI method is used to solve the MOP, using Eq. 33.
- Step 4. Mixture design definition: In order to set the weights to be used in the optimization routine described in Step 3, a mixture design is done using Minitab® 16.
- Step 5. MOP solution: The optimization problem of step 3 is solved for each experimental condition defined in step 4.
- Step 6. Calculation of weighting metrics and UPV: Weighting metric ξ , *Entropy*, and *GPE* are obtained using, respectively, Eqs. 34, 35, and 36, and UPV is equal to $\mathbf{X}_0^T(\mathbf{X}^T\mathbf{X})^{-1}\mathbf{X}_0$.
- Step 7. Metrics modeling: The canonical polynomial of mixtures is calculated for described metrics using the step 6 calculation results.
- Step 8. Optimal weights definition: The metric that leads to the response with the smallest variance is used in order to achieve the optimal weights.

As algorithms are used for the solution of MOP, the limitations inherent in these algorithms will always be present. In the current study, the generalized reduced gradient (GRG) algorithm is used by the Excel® Solver function to solve the problem.

6 Results and discussions

The analysis of experimental data shown in Table 2 generated the mathematical modeling presented in Table 3.

The models' adequacy has been checked with the ANOVA. When the null hypothesis (H_0) is rejected, it means that at least one of the decision variables contributes significantly to the function [32, 33]. In ANOVA, small p values are desirable. The p values for the analyzed objective functions show a statistically significant regression at 5 % level of significance, proving the functions' adequacy. On the terms, it draws attention the statistical significance of the interaction terms $V_c \times f$, $V_c \times d$, and $f \times d$. It proves the synergistic effect between cutting speed (V_c), feed rate (f), and depth of cut (d) in the productivity parameter MRR/F_c .

The coefficient of multiple determination (R^2) represents the percentage of the observed data in the response that can be explained by the mathematical model. In this case, R^2 values show that the models have a good adjustment. The T has shown the worst R^2 , 90.56 %. Even so, this value is considered acceptable [32, 33].

In order to compare how each decision variable affects each response, the main effect plots for T , R_a , and MRR/F_c are shown in Fig. 5.

According to this analysis, V_c is the most significant factor in decreasing T . V_c is also an important factor when analyzing MRR/F_c , but in an opposite way. By increasing the V_c , the MRR/F_c is increased. The behavior of these responses related to the variation in V_c shows the conflicting nature of the objectives. Seeking to increase productivity, an increase in V_c values can drastically decrease the T , increasing the process cost, since the price of the cutting tool is very significant for the cost of operation. Concerning to R_a , the larger V_c , the smaller the R_a . This result is in accordance to that presented by other authors when turning other hard materials with wiper tools [3, 10, 30]. The variable f is the most significant for R_a

Table 1 Parameters used in the experiments

Factors	Symbol	Levels				
		-1.682	-1	0	1	1.682
Cutting speed (m/min)	V_c	57.38	100	162.5	225	267.62
Feed rate (mm/rev)	f	0.06	0.10	0.16	0.22	0.26
Depth of cut (mm)	d	0.09	0.15	0.24	0.33	0.39

Table 2 CCD for T , Ra , and MRR/Fc

Number	V_c (m/min)	f (mm/rev)	d (mm)	T (min)	Ra (μm)	MRR/Fc ($\text{cm}^3/\text{N min}$)
1	-1	-1	-1	70.00	0.13	0.00438
2	+1	-1	-1	35.00	0.09	0.01416
3	-1	+1	-1	57.00	0.52	0.00778
4	+1	+1	-1	32.50	0.26	0.03115
5	-1	-1	+1	67.00	0.14	0.00739
6	+1	-1	+1	33.00	0.12	0.03011
7	-1	+1	+1	55.00	0.48	0.01634
8	+1	+1	+1	31.50	0.45	0.06725
9	-1.682	0	0	63.00	0.29	0.00450
10	+1.682	0	0	28.25	0.15	0.04608
11	0	-1.682	0	42.50	0.12	0.00687
12	0	+1.682	0	44.50	0.54	0.02879
13	0	0	-1.628	54.50	0.15	0.00703
14	0	0	+1.682	51.50	0.15	0.02822
15	0	0	0	46.50	0.15	0.01871
16	0	0	0	45.50	0.16	0.01881
17	0	0	0	47.50	0.14	0.01877
18	0	0	0	47.00	0.17	0.01888
19	0	0	0	46.50	0.16	0.01869

variation similar to the results described by Paiva et al. [10]. By increasing the f above 0.16 mm/rev, Ra increases considerably which shows that even for a tool with wiper geometry f cannot be increased discretionarily. When analyzing only f , it is observed that in order to increase MRR/Fc , Ra would be jeopardized. Regarding the variable d , its influence is higher to MRR/Fc . When using the maximum value of d , the values of T and MRR/Fc increase and Ra decreases, making it clear that there is no conflict between the responses to this variable, since the aim is to maximize T and MRR/Fc and to minimize Ra .

Table 3 Mathematical models for objective functions

Terms	T (min)	Ra (μm)	MRR/Fc ($\text{cm}^3/\text{N min}$)
Constant	46.592	0.155	0.01870
V_c	-12.846	-0.042	0.01294
f	-1.877	0.142	0.00757
d	-0.955	0.014	0.00727
V_c^2	-0.301	0.030	0.00273
f^2	-1.053	0.069	0.00009
d^2	2.306	0.005	0.00002
$V_c \times f$	2.625	-0.029	0.00522
$V_c \times d$	0.250	0.031	0.00506
$f \times d$	0.250	0.014	0.00321
p Value	0.000	0.000	0.000
Adjusted R^2 (%)	90.56 %	92.71 %	97.21 %

Values in bold represent significant terms in the model (p value $< 5\%$)

Figure 6 shows the response surfaces for T , Ra , and MRR/Fc .

Figure 6 confirms the conflicting nature of the objectives. While an increase in V_c causes an increase in MRR/Fc , it causes a decrease in T . Moreover, an increase in f causes an increase in MRR/Fc and it causes an increase in Ra .

In order to check the functions' convexity, before performing the multiobjective optimization, the nature of the stationary point is analyzed by using Eq. 30. For T , the eigenvalues (λ_i) are [2.3249; -2.0424; 0.6696], i.e., the different eigenvalue signs indicate that the function is neither concave nor convex and the stationary point is a saddle point. For Ra , the eigenvalues (λ_i) are [0.0739; 0.0348; 0.0046], i.e., the positive signs of eigenvalues indicate that the function is convex and the stationary point is a point of minimum. For MRR/Fc , the eigenvalues (λ_i) are [0.0059; -0.0016; -0.0015], i.e., the different eigenvalues signs indicate that the function is neither concave nor convex and the stationary point is a saddle point. The analysis of the nature of the stationary point reveals that the functions have different convexities and, because of that, the weighted sum method for multiobjective optimization is not the most suitable, according to Das and Dennis [41]. Thus, in this work, the NBI method is used. It is important to mention that Tables 1 and 3 are equivalent to steps 1 and 2 of the multiple criteria decision-making process, respectively, being the NBI method used in step 3,

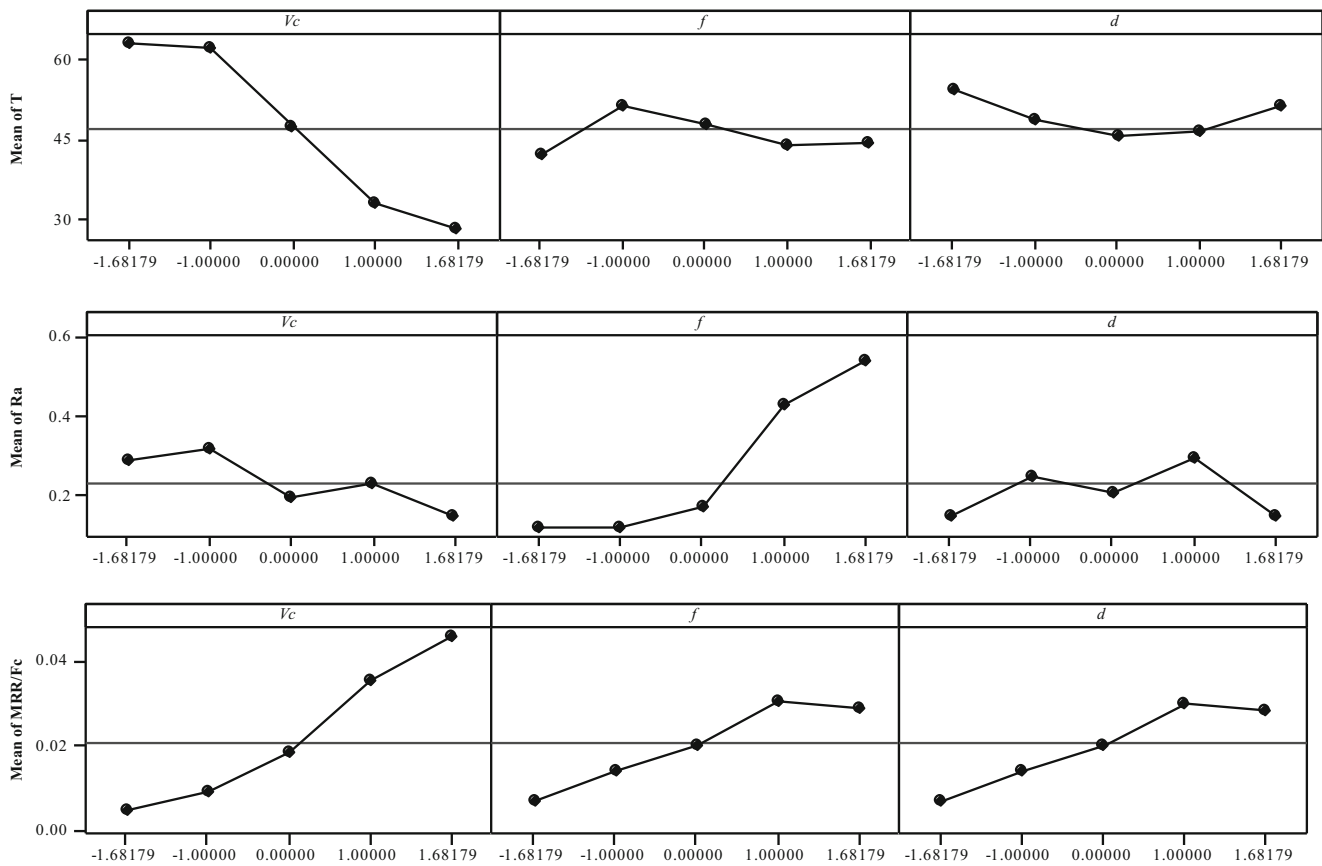


Fig. 5 Main effect plots for T , Ra , and MRR/Fc

MOP formulation, as described in Sect. 5. To implement the optimization routine described in step 3, initially, the payoff matrix was estimated obtaining the results reported in Table 4.

The results in Table 4 are obtained by the individual maximization of the mathematical models for T , Ra , and MRR/Fc . It is possible to see that in the MRR/Fc maximum response, T and Ra values are the worst ones.

Once step 3 has been implemented, a mixture design for the weights of each objective function (step 4) was defined. Subsequently, the solution of the optimization problem of step 3 was obtained for each experimental condition defined by the mixture design (step 5). Based on these results, weighting metric ξ and UPV have been calculated (step 6). The results are shown in Table 5, where w_1 , w_2 , and w_3 are the weights of T , Ra , and MRR/Fc , respectively.

The results presented in Table 5 comprise the Pareto optimal set for the multiobjective problem. By changing the weights or the degree of importance assigned to each response, the results of the optimization process are altered, favoring the response with the highest weight. The utilization of MDE along with the NBI method makes it easier to define a Pareto frontier with

evenly distributed solutions, regardless of the convexity of the functions. Once again, it is clear that the conflicting nature of the responses as T and MRR/Fc are negatively affected when minimizing Ra . Regarding the values of UPV, it is important to note that the values are changed with the change in the results of the optimization process, i.e., the prediction variance behavior is related to the weighting. This result confirms that the robustness of the optimization process is associated with the choice of the Pareto optimal point as the final solution for the MOP. Table 6 presents an analysis using Pearson correlation between the values of the metrics presented in Table 5. p Values less than 5 % indicate statistically significant correlations.

The Pearson correlation analysis showed that the weighting metric ξ has negative and statistically significant correlation with UPV, i.e., by maximizing this metric, the variance values tend to be lower. This information provides us with evidence that the search for the most preferred Pareto optimal point in multiobjective optimization using this metric leads to a robust response from the variability point of view.

Step 7 involves the modeling of metrics from the data presented in Figs. 7, 8, 9, and 10 and Table 5.

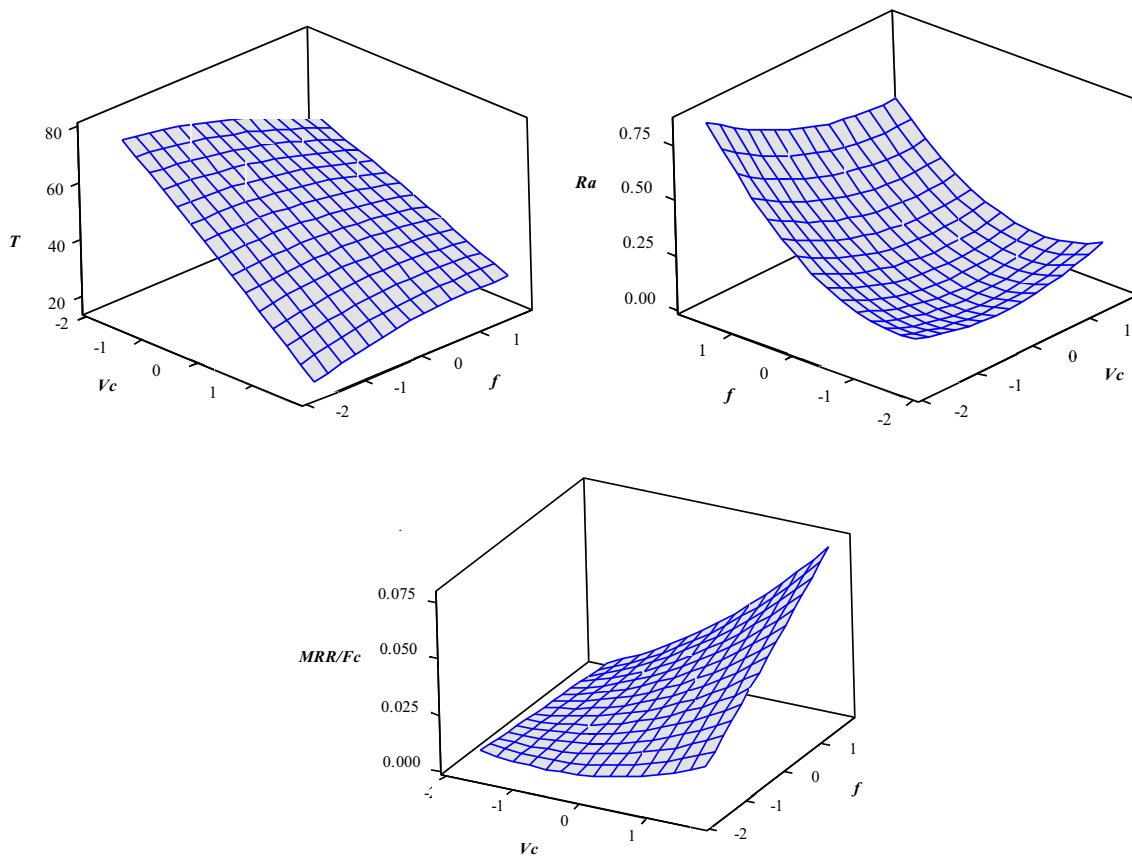


Fig. 6 Response surface for T , Ra , and MRR/Fc (hold value: $d = 0$)

Thus, their canonical polynomials of mixture, response surfaces, and contour plots are as follows:

$$\begin{aligned}
 \text{Entropy} = & -0.0074w_1 - 0.0074w_2 - 0.0074w_3 \\
 & + 2.7705w_1w_2 + 2.7705w_1w_3 \\
 & + 2.7705w_2w_3 + 5.4207w_1w_1w_2w_3 \\
 & + 5.4207w_1w_2w_2w_3 + 5.4207w_1w_2w_3w_3 \\
 & + 1.4619w_1w_2(w_1-w_2)^2 \\
 & + 1.4619w_1w_3(w_1-w_3)^2 \\
 & + 1.4619w_2w_3(w_2-w_3)^2
 \end{aligned} \tag{38}$$

Table 4 Payoff matrix for the objective functions

T	Ra	MRR/Fc
69.5370	0.2267	0.0064
39.5259	0.0613	0.0118
31.0776	0.3251	0.0633

Bold values represent individual optimums

$$\begin{aligned}
 GPE = & 3.6073w_1 + 1.2343w_2 + 4.8560w_3 \\
 & + 0.3807w_1w_3(w_1-w_3) - 2.3481w_1w_1w_2w_3 \\
 & + 0.9104w_1w_2w_2w_3 + 1.0900w_1w_2w_3w_3 \\
 & + 0.6818w_1w_3(w_1-w_3)^2
 \end{aligned} \tag{39}$$

$$\begin{aligned}
 \xi = & -0.0047w_1 + 0.0144w_2 - 0.0077w_3 + 1.1146w_1w_2 \\
 & + 0.6686w_1w_3 \\
 & + 0.8752w_2w_3 - 0.6308w_1w_2(w_1-w_2) \\
 & + 0.0866w_1w_3(w_1-w_3) + 0.6337w_2w_3(w_2-w_3) \\
 & + 1.8988w_1w_1w_2w_3 + 1.1581w_1w_2w_2w_3 \\
 & + 0.8336w_1w_2w_3w_3 + 0.8713w_1w_2(w_1-w_2)^2 \\
 & + 0.3672w_1w_3(w_1-w_3)^2 + 0.9321w_2w_3(w_2-w_3)^2
 \end{aligned} \tag{40}$$

Table 5 Mixture design

Weights			T	Ra	MRR/Fc	$Entropy$	GPE	ξ	UPV
w_1	w_2	w_3							
1.000	0.000	0.000	69.5370	0.2267	0.0064	0.0000	3.5992	0.0000	0.6073
0.900	0.100	0.000	67.2736	0.2102	0.0069	0.3251	3.3531	0.0969	0.5258
0.900	0.000	0.100	65.6911	0.2366	0.0065	0.3251	3.8135	0.0852	0.4173
0.800	0.200	0.000	63.5348	0.1936	0.0068	0.5004	3.1380	0.1595	0.3095
0.800	0.100	0.100	62.6900	0.2200	0.0068	0.6390	3.5809	0.1785	0.2724
0.800	0.000	0.200	61.8451	0.2464	0.0108	0.5004	3.9604	0.1263	0.6073
0.700	0.300	0.000	60.5337	0.1771	0.0080	0.6109	2.8928	0.2112	0.2347
0.700	0.200	0.100	59.6889	0.2035	0.0132	0.8018	3.2542	0.2464	0.4513
0.700	0.100	0.200	58.8440	0.2299	0.0173	0.8018	3.6310	0.2208	0.6073
0.700	0.000	0.300	56.0302	0.2562	0.0234	0.6109	4.0053	0.1525	0.6073
0.600	0.400	0.000	57.5326	0.1605	0.0086	0.6730	2.6574	0.2533	0.1950
0.600	0.300	0.100	56.6877	0.1869	0.0137	0.8979	3.0188	0.2975	0.2442
0.600	0.200	0.200	55.8430	0.2133	0.0188	0.9503	3.3801	0.2811	0.3627
0.600	0.100	0.300	54.9981	0.2397	0.0240	0.8979	3.7415	0.2400	0.5131
0.600	0.000	0.400	54.1533	0.2661	0.0277	0.6730	4.1261	0.1631	0.6073
0.500	0.500	0.000	54.5315	0.1440	0.0091	0.6931	2.4220	0.2862	0.1990
0.500	0.400	0.100	53.6866	0.1704	0.0142	0.9433	2.7833	0.3389	0.1870
0.500	0.300	0.200	52.8418	0.1968	0.0194	1.0297	3.1447	0.3274	0.2206
0.500	0.200	0.300	51.9970	0.2232	0.0245	1.0297	3.5061	0.2937	0.2969
0.500	0.100	0.400	51.1522	0.2495	0.0297	0.9433	3.8674	0.2439	0.4069
0.500	0.000	0.500	50.3073	0.2759	0.0348	0.6931	4.2288	0.1639	0.5460
0.400	0.600	0.000	51.5303	0.1275	0.0096	0.6730	2.1865	0.3078	0.2320
0.400	0.500	0.100	50.6856	0.1538	0.0148	0.9433	2.5479	0.3702	0.1933
0.400	0.400	0.200	49.8407	0.1802	0.0199	1.0549	2.9093	0.3626	0.1860
0.400	0.300	0.300	48.9959	0.2066	0.0251	1.0889	3.2706	0.3329	0.2048
0.400	0.200	0.400	48.1511	0.2330	0.0302	1.0549	3.6320	0.2905	0.2580
0.400	0.100	0.500	47.3062	0.2594	0.0354	0.9433	3.9934	0.2362	0.3437
0.400	0.000	0.600	46.4614	0.2858	0.0405	0.6730	4.3547	0.1545	0.4601
0.300	0.700	0.000	48.5292	0.1109	0.0102	0.6109	1.9511	0.3131	0.3613
0.300	0.600	0.100	47.6844	0.1373	0.0153	0.8979	2.3124	0.3883	0.1931
0.300	0.500	0.200	46.8396	0.1637	0.0205	1.0297	2.6738	0.3851	0.1951
0.300	0.400	0.300	45.9948	0.1901	0.0256	1.0889	3.0352	0.3588	0.1860
0.300	0.300	0.400	45.1500	0.2164	0.0308	1.0889	3.3965	0.3206	0.1988
0.300	0.200	0.500	44.3051	0.2428	0.0359	1.0297	3.7579	0.2740	0.2413
0.300	0.100	0.600	43.4603	0.2692	0.0411	0.8979	4.1193	0.2180	0.3151
0.300	0.000	0.700	42.6155	0.2956	0.0462	0.6109	4.4806	0.1363	0.4202
0.200	0.800	0.000	45.5281	0.0944	0.0111	0.5004	1.7103	0.2926	0.6073
0.200	0.700	0.100	44.6833	0.1208	0.0159	0.8018	2.0770	0.3860	0.1886
0.200	0.600	0.200	43.8385	0.1471	0.0210	0.9503	2.4384	0.3897	0.1962
0.200	0.500	0.300	42.9937	0.1735	0.0262	1.0297	2.7997	0.3678	0.1908
0.200	0.400	0.400	42.1488	0.1999	0.0313	1.0549	3.1611	0.3337	0.1863
0.200	0.300	0.500	41.3040	0.2263	0.0365	1.0297	3.5225	0.2923	0.2016
0.200	0.200	0.600	40.4592	0.2527	0.0416	0.9503	3.8838	0.2447	0.2443
0.200	0.100	0.700	39.6143	0.2791	0.0468	0.8018	4.2452	0.1889	0.3175
0.200	0.000	0.800	38.7695	0.3054	0.0519	0.5004	4.6066	0.1086	0.4230
0.100	0.900	0.000	42.5270	0.0778	0.0113	0.3251	1.4802	0.2196	0.2657
0.100	0.800	0.100	41.6822	0.1042	0.0164	0.6390	1.8415	0.3470	0.3002
0.100	0.700	0.200	40.8374	0.1306	0.0216	0.8018	2.2029	0.3640	0.1862

Table 5 (continued)

Weights			<i>T</i>	<i>Ra</i>	<i>MRR/Fc</i>	<i>Entropy</i>	<i>GPE</i>	ξ	<i>UPV</i>
<i>w</i> ₁	<i>w</i> ₂	<i>w</i> ₃							
0.100	0.600	0.300	39.9926	0.1570	0.0267	0.8979	2.5643	0.3502	0.1878
0.100	0.500	0.400	39.1477	0.1834	0.0319	0.9433	2.9256	0.3224	0.1860
0.100	0.400	0.500	38.3029	0.2097	0.0370	0.9433	3.2870	0.2870	0.1924
0.100	0.300	0.600	37.4581	0.2361	0.0422	0.8979	3.6484	0.2461	0.2190
0.100	0.200	0.700	36.6132	0.2625	0.0473	0.8018	4.0098	0.2000	0.2728
0.100	0.100	0.800	35.7684	0.2889	0.0525	0.6390	4.3711	0.1462	0.3577
0.100	0.000	0.900	34.9236	0.3153	0.0576	0.3251	4.7325	0.0687	0.4766
0.000	1.000	0.000	39.5259	0.0613	0.0118	0.0000	1.2447	0.0000	0.6073
0.000	0.900	0.100	38.6811	0.0842	0.0170	0.3251	1.5495	0.2098	0.6073
0.000	0.800	0.200	37.8363	0.1140	0.0221	0.5004	1.9675	0.2543	0.2612
0.000	0.700	0.300	36.9914	0.1404	0.0273	0.6109	2.3288	0.2623	0.1963
0.000	0.600	0.400	36.1466	0.1668	0.0324	0.6730	2.6902	0.2502	0.1918
0.000	0.500	0.500	35.3018	0.1932	0.0376	0.6931	3.0516	0.2271	0.2000
0.000	0.400	0.600	34.4569	0.2196	0.0427	0.6730	3.4129	0.1972	0.2242
0.000	0.300	0.700	33.6121	0.2460	0.0479	0.6109	3.7743	0.1618	0.2720
0.000	0.200	0.800	32.7673	0.2723	0.0530	0.5004	4.1357	0.1210	0.3490
0.000	0.100	0.900	31.9225	0.2987	0.0582	0.3251	4.4970	0.0723	0.4597
0.000	0.000	1.000	31.0776	0.3251	0.0633	0.0000	4.8584	0.0000	0.6073
0.333	0.333	0.333	46.7135	0.2044	0.0272	1.0986	3.2341	0.3397	0.1919
0.667	0.167	0.167	58.1253	0.2155	0.0168	0.8676	3.4166	0.2539	0.4824
0.167	0.667	0.167	43.1197	0.1328	0.0195	0.8676	2.2394	0.3874	0.1880
0.167	0.167	0.667	38.8955	0.2647	0.0452	0.8676	4.0463	0.2144	0.2720

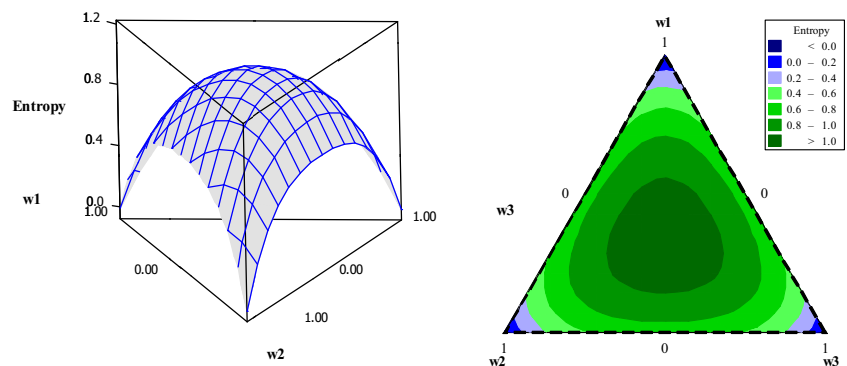
Table 6 Pearson correlation

	<i>Entropy</i>	<i>GPE</i>	ξ
<i>GPE</i>	-0.003	0.980	
ξ	0.803	-0.530	0.000
<i>UPV</i>	-0.635	0.312	-0.715
	0.057	0.008	0.000

$$UPV = 0.4942w_1 + 0.5877w_2 + 0.5683w_3 - 1.2329w_1w_2 - 1.5102w_2w_3 + 1.1778w_1w_3(w_1 - w_3) - 4.1337w_1w_2w_3 \quad (41)$$

It should be noted that all canonical polynomials of mixture had good fitness, since almost all have *R*² close to 100 %. The metric of variance, UPV, has shown the worst *R*², 79.66 %. Even so, this value is considered acceptable [32, 33]. Something that draws attention in this analysis is the fact that it was possible to model the

Fig. 7 Entropy response surface and contour plot



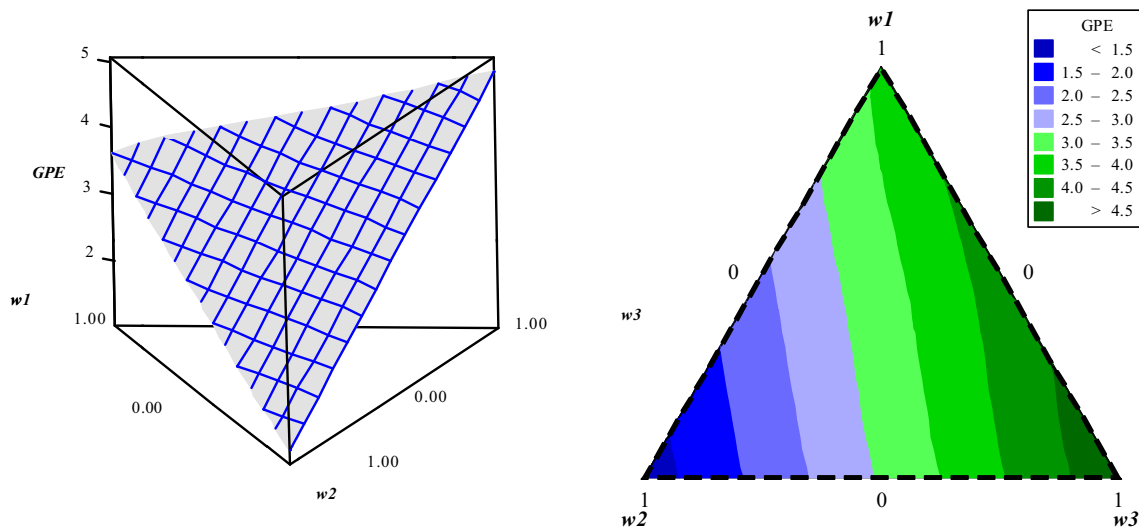


Fig. 8 GPE response surface and contour plot

metric of variance, UPV, in terms of weights. This is because the weights interfere in the solution space. However, since optimization of distinct functions are performed simultaneously, the solution space is not the same initial area of the DOE and therefore, when modeling the variance, its shape is distinguished from the hat matrix shape.

Lastly, step 8 was executed. By the maximization of ξ , described in Eq. 40, the weights w_1 , w_2 , and w_3 , related to the final solution were found. The values are $w_1 = 0.2352$, $w_2 = 0.5942$, and $w_3 = 0.1706$. These optimal weights were used in a multiobjective optimization of T , Ra , and MRR/Fc , reaching the values of 45.1426 min, 0.1452 μm , and 0.0193 $\text{cm}^3/\text{N min}$,

respectively. This result is considered acceptable when comparing it to the results regarding other hardened steels reported in literature [4–16, 30]. The optimal coded values of the decision variables are $V_c = 0.1250$, $f = -0.0193$, and $d = -0.1109$. The coded values were transformed in uncoded values by the use of Eq. 37. Thus, the optimal values of decision variables are $V_c = 170.3116 \text{ m/min}$, $f = 0.1588 \text{ mm/rev}$, and $d = 0.2300 \text{ mm}$.

Figure 11 shows the Pareto frontier built using the NBI method, with the optimal highlighted. The data presented in Table 5 have been used to build Fig. 11.

In Fig. 11, it has been shown that the Pareto optimal points on the frontier are evenly distributed. Moreover, we can find

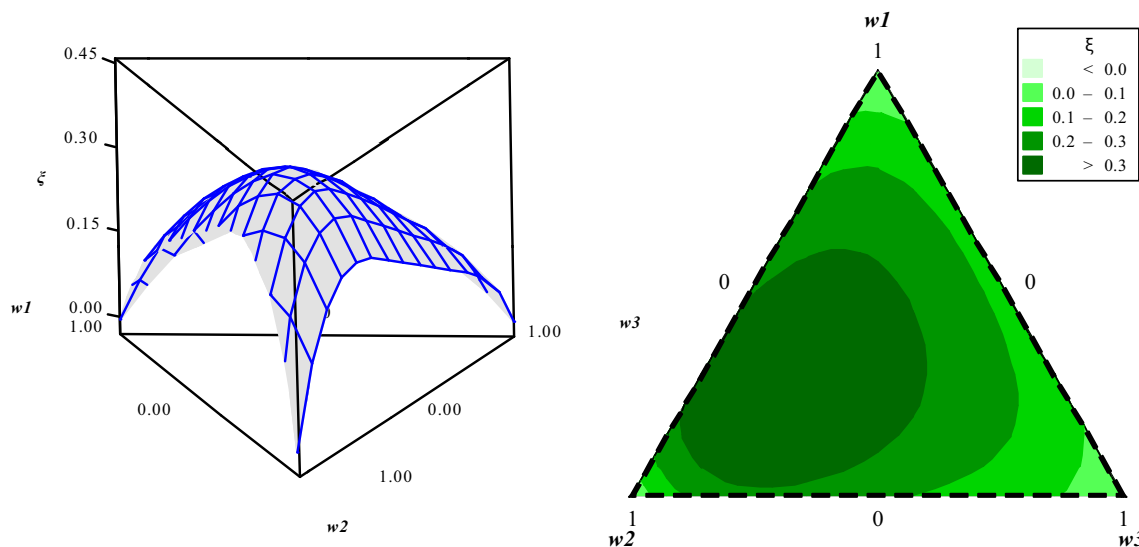


Fig. 9 ξ response surface and contour plot

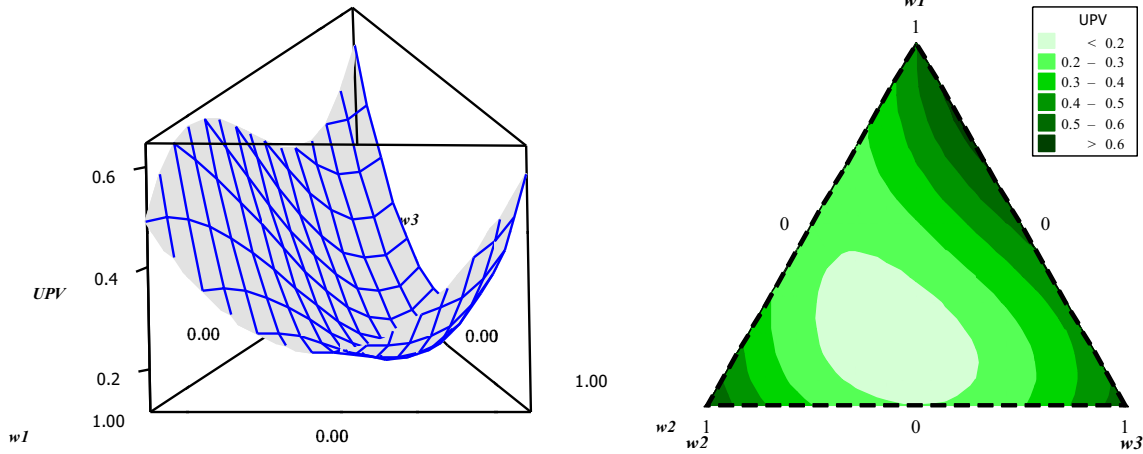


Fig. 10 UPV response surface and contour plot

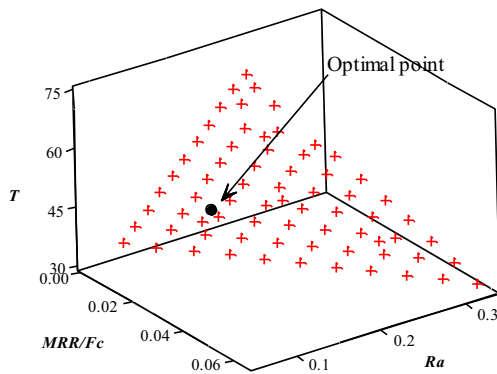


Fig. 11 Pareto frontier for T , Ra , and MRR/Fc

in Fig. 11 the most preferred Pareto optimal point, as the final solution for the MOP. Table 7 shows the confidence intervals for the responses associated to the optimal point. Equation 15 is used, and the adopted probability is 95 %, i.e., $\alpha=5\%$.

From the variability point of view, the final solution obtained with the maximization of ξ metric is the robust one, since this metric leads the solution to a region of minimum variance, less variability, and greater reliability. However, the confidence interval of Ra is higher than the other responses. It proves that Ra is the most difficult parameter to control in the analyzed process.

Figure 12 shows the overlap of the different objective functions defining the feasible region for the problem.

Table 7 Confidence intervals

Responses	Lower limit	Mean	Upper limit
T	41.4313	45.1426	48.8539
Ra	0.1045	0.1452	0.1860
MRR/Fc	0.0167	0.0193	0.0220

Figure 12 shows the conflicting nature between MRR/Fc and the other responses. An increase in MRR/Fc leads to a decrease in T and to an increase in Ra . In this work, the optimal point was chosen based on the maximization of ξ metric and it has been proved that this point is the robust one.

7 Conclusions

In this paper, the process of AISI H13 hardened steel turning with PCBN wiper tool was analyzed. The NBI method was used to simultaneously optimize tool life (T), surface roughness parameter (Ra), and the ratio between material removal rate and cutting force (MRR/Fc). By using this method, it was possible to build an evenly distributed Pareto frontier for the three responses, regardless the functions convexity.

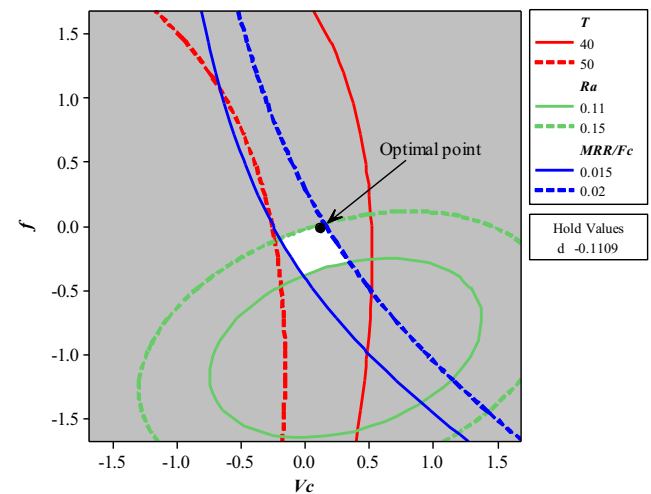


Fig. 12 Point of optimization for T , Ra , and MRR/Fc

The mathematical model for responses presented an acceptable fitting proving the functions adequacy. Some relevant results were obtained as follows: it has been shown the synergistic effect between cutting speed (V_c), feed rate (f), and depth of cut (d) in the productivity parameter MRR/F_c ; the variable V_c has been identified as the most significant factor in decreasing T ; the variable f has been identified as the most significant for R_a variation, though V_c be also significant; the variable V_c has been identified as the most significant factor in increasing MRR/F_c , though f be also significant; and, among the analyzed responses, d is a significant factor only for MRR/F_c .

An entropic measure, the weighting metric ξ , was used to select the most preferred Pareto optimal point as the final solution. These decision-making criteria proved to be useful in mapping regions of minimum variance within the Pareto optimal responses obtained in the optimization process. Thus, the study was able to demonstrate that the weights used in the multiobjective optimization process influence the prediction variance of obtained response. Furthermore, the study was able to prove the robustness of the multiple criteria decision making employed to choose the final solution. It is noticed that the benefits of this weighting based in entropy is even more useful in estimated models, such as surface models, because it reduces the forecast error.

The simultaneous optimal values for the objective functions are $T = 45.1426$ min, $R_a = 0.1452$ μm , and $MRR/F_c = 0.0193$ $\text{cm}^3/\text{N min}$. Such results were obtained with the following combination of process parameters: $V_c = 170.3116$ m/min, $f = 0.1588$ mm/rev, and $d = 0.2300$ mm. Analyzing the responses' confidence interval, the R_a has greater variability being the most difficult parameter to control in the analyzed process.

Acknowledgments The authors would like to thank the Brazilian Government agencies CNPq, CAPES, FAPEMIG, and IFULDEMINAS for their support.

Compliance with ethical standards

Conflict of interest The authors declare that they have no conflict of interest.

References

- König W, Berkold A, Koch KF (1993) Turning versus grinding—a comparison of surface integrity aspects and attainable accuracies. *Annals of the CIRP* 42(1):39–43
- Tönshoff HK, Arendt C, Ben Amor R (2000) Cutting of hardened steel. *Annals of the CIRP* 49(2):547–566
- Özel T, Karpat Y, Figueira L, Davim JP (2007) Modelling of surface finish and tool flank wear in turning of AISI D2 steel with ceramic wiper inserts. *J Mater Process Technol* 189(1–3):192–198
- Gaitonde VN, Karnik SR, Figueira L, Davim JP (2009) Machinability investigations in hard turning of AISI D2 cold work tool steel with conventional and wiper ceramic inserts. *Int J Refract Met Hard Mater* 27(4):754–763
- Bouacha K, Yallese MA, Mabrouki T, Rigal JF (2010) Statistical analysis of surface roughness and cutting forces using response surface methodology in hard turning of AISI 52100 bearing steel with CBN tool. *Int J Refract Met Hard Mater* 28(3):349–361
- Mandal N, Doloi B, Mondal B (2011) Development of flank wear prediction model of zirconia toughened alumina (ZTA) cutting tool using response surface methodology. *Int J Refract Met Hard Mater* 29(2):273–280
- Grzesik W (2009) Wear development on wiper Al₂O₃-TiC mixed ceramic tools in hard machining of high strength steel. *Wear* 266(9–10):1021–1028
- Paiva AP, Ferreira JR, Balestrassi PP (2007) A multivariate hybrid approach applied to AISI 52100 hardened steel turning optimization. *J Mater Process Technol* 189(1–3):26–35
- Paiva AP, Paiva EJ, Ferreira JF, Balestrassi PP, Costa SC (2009) A multivariate mean square error optimization of AISI 52100 hardened steel turning. *Int J Adv Manuf Technol* 43(7):631–643
- Paiva AP, Campos PH, Ferreira JR, Lopes LGD, Paiva EJ, Balestrassi PP (2012) A multivariate robust parameter design approach for optimization of AISI 52100 hardened steel turning with wiper mixed ceramic tool. *Int J Refract Met Hard Mater* 30:152–163
- Huang Y, Chou YK, Liang SY (2007) CBN tool wear in hard turning: survey on research progresses. *Int J Adv Manuf Technol* 35(5):443–453
- Tamizharasan T, Sevaraj T, Haq AN (2006) Analysis of tool wear and surface finish in hard turning. *Int J Adv Manuf Technol* 28(7):671–679
- Singh D, Rao PV (2007) A surface roughness model for hard turning process. *Int J Adv Manuf Technol* 32(11):1115–1124
- Özel T, Hsu TK, Zeren E (2005) Effects of cutting edge geometry, workpiece hardness, feed rate and cutting speed on surface roughness and forces in finish turning of hardened AISI H13 steel. *Int J Adv Manuf Technol* 25(3):262–269
- Lima JG, Ávila RF, Abrão AM, Faustino M, Davim JP (2005) Hard turning: AISI 4340 high strength low alloy steel and AISI D2 cold work tool steel. *J Mater Process Technol* 169(3):388–395
- Diniz AE, Ferreira JR, Filho FT (2003) Influence of refrigeration/lubrication condition on SAE 52100 hardened steel turning at several cutting speeds. *The International Journal of Machine Tools and Manufacture* 42(3):317–326
- Iqbal A, Ning H, Khan I, Liang L, Dar NU (2008) Modeling the effects of cutting parameters in MQL-employed finish hard-milling process using D-optimal method. *J Mater Process Technol* 199(1–3):379–390
- Zhou JM, Andersson M, Stahl JE (2003) The monitoring of flank wear on the CBN tool in the hard turning process. *Int J Adv Manuf Technol* 22(9):697–702
- Quiza R, Figueira L, Davim JP (2008) Comparing statistical models and artificial neural networks on predicting the tool wear in hard machining D2 AISI steel. *Int J Adv Manuf Technol* 37(7):641–648
- Singh D, Rao PV (2008) Performance improvement of hard turning with solid lubricants. *Int J Adv Manuf Technol* 38(5):529–535
- Bouacha K, Yallese MA, Khamel S, Belhadi S (2014) Analysis and optimization of hard turning operation using cubic boron nitride tool. *International Journal of Refractory Metals & Hard Materials* 45:160–178

22. Lahiff C, Gordon S, Phelan P (2007) PCBN tool wear modes and mechanisms in finish hard turning. *Robot Comput Integr Manuf* 23(6):638–644
23. Poulachon G, Moisan A, Jawahir IS (2001) Tool-wear mechanisms in hard turning with polycrystalline cubic boron nitride tools. *Wear* 250(1–12):576–586
24. Harris TK, Brookes EJ, Taylor CJ (2004) The effect of temperature on the hardness of polycrystalline cubic boron nitride cutting tool materials. *Int J Refract Met Hard Mater* 22(2–3):105–110
25. Angseryd J, Elfving M, Olsson E, Andrén HO (2009) Detailed microstructure of a cBN based cutting tool material. *Int J Refract Met Hard Mater* 27(2):249–255
26. Heath PJ (1986) Properties and uses of amborite. *Ind Diam Rev* 46(514):120–127
27. König W, Tönshoff HK, Ackershoff G (1984) Machining of hard materials. *Annals of the CIRP* 33(2):417–427
28. Brookes CA (1986) The mechanical properties of cubic boron nitride—a perspective view. *Inst Phys Conf Ser* 75:207–220
29. Herzog DE (1977) Cutting tools with COMPAX diamond and BZN compact inserts slash production time and lower part cost. *Cutting Tool Engineering* 5:64–67
30. Correia AE, Davim JP (2011) Surface roughness measurement in turning carbon steel AISI 1045 using wiper inserts. *Measurement* 44(5):1000–1005
31. Anderson-Cook CM, Borror CM, Montgomery DC (2009) Response surface design evaluation and comparison. *Journal of Statistical Planning and Inference* 139(2):629–641
32. Montgomery DC (2001) *Design and analysis of experiments*, 5 edn. John Wiley & Sons, New York
33. Myers RH, Montgomery DC, Anderson-Cook CM (2009) *Response surface methodology: process and product optimization using designed experiments*, 3 edn. Wiley, New York
34. Box GEP, Draper NR (1987) *Empirical model-building and response surfaces*. Wiley, New York
35. Cornell J (2002) *Experiments with mixtures: designs, models, and the analysis of mixture data*, third edn. Wiley, New York
36. Miettinen K (1999) *Nonlinear multiobjective optimization*. Kluwer Academic Publishers, Boston
37. Baril C, Yacout S, Clément B (2011) Design for Six Sigma through collaborative multiobjective optimization. *Comput Ind Eng* 60(1):43–55
38. Shahrafi AF, Noorossana R (2014) Reliability-based robust design optimization: a general methodology using genetic algorithm. *Comput Ind Eng* 74:199–207
39. Hwang CL, Masud ASM (1979) Multiple objective decision making—methods and applications: a state-of-the-art survey, vol. 164 of *Lecture Notes in Economics and Mathematical Systems*. Springer, Berlin
40. Zhang W, Yang H (2001) A study of the weighting method for a certain type of multicriteria optimization problem. *Comput Struct* 79(31):2741–2749
41. Das I, Dennis JE (1997) A closer look at drawbacks of minimizing weighted sums of objectives for Pareto set generation in multicriteria optimization problems. *Structural Optimization* 14(1):63–69
42. Shin S, Samanlioglu F, Cho BR, Wiecek MM (2011) Computing trade-offs in robust design: perspectives of the mean squared error. *Comput Ind Eng* 60(2):248–255
43. Vahidinasab V, Jadid S (2010) Normal boundary intersection method for suppliers' strategic bidding in electricity markets: an environmental/economic approach. *Energy Convers Manag* 51(6):1111–1119
44. Das I, Dennis JE (1998) Normal boundary intersection: a new method for generating the Pareto surface in nonlinear multicriteria optimization problems. *SIAM J Optim* 8(3):631–657
45. Utyuzhnikov SV, Fantini P, Guenov MD (2009) A method for generating a well-distributed Pareto set in nonlinear multiobjective optimization. *J Comput Appl Math* 223(2):820–841
46. Shukla PK, Deb K (2007) On finding multiple Pareto-optimal solutions using classical and evolutionary generating methods. *Eur J Oper Res* 181(3):1630–1652
47. Jia Z, Ierapetritou G (2007) Generate Pareto optimal solutions of scheduling problems using normal boundary intersection technique. *Comput Chem Eng* 31(4):268–280
48. Mela K, Tiainen T, Heinisuo M, Baptiste P (2012) Comparative study of multiple criteria decision making methods for building design. *Adv Eng Inform* 26:716–726
49. Szeląg M, Greco S, Słowiński R (2014) Variable consistency dominance-based rough set approach to preference learning in multicriteria ranking. *Inf Sci* 277(1):525–552
50. Ibáñez-Forés V, Bovea MD, Pérez-Belis V (2014) A holistic review of applied methodologies for assessing and selecting the optimal technological alternative from a sustainability perspective. *J Clean Prod* 70(1):259–281
51. Taboada HA, Baheranwala F, Coit DW, Wattanapongsakorn N (2007) Practical solutions for multi-objective optimization: an application to system reliability design problems. *Reliab Eng Syst Saf* 92(3):314–322
52. Gaudreault C, Samson R, Stuart P (2009) Implications of choices and interpretation in LCA for multi-criteria process design: deinked pulp capacity and cogeneration at a paper mill case study. *J Clean Prod* 17(17):1535–1546
53. Pilavachi PA, Stephanidis SD, Pappas VA, Afgan NH (2009) Multi-criteria evaluation of hydrogen and natural gas fuelled power plant technologies. *Appl Therm Eng* 29(11–12):2228–2234
54. Figueira JR, Greco S, Słowiński R (2009) Building a set of additive value functions representing a reference preorder and intensities of preference: GRIP method. *Eur J Oper Res* 195(2):460–486
55. Zeleny M (1974) A concept of compromise solutions and the method of the displaced ideal. *Comput Oper Res* 1(3–4):479–496
56. Zeleny M (1975) The theory of the displaced ideal. In: Zeleny M (ed) *Lecture notes in economics and mathematical systems*, 123: multiple criteria decision making - Kyoto. Springer-Verlag, Berlin
57. Rocha LCS, Paiva AP, Balestrassi PP, Severino G, Rotela Junior P (2015a) Entropy-based weighting for multiobjective optimization: an application on vertical turning. *Math Probl Eng*, 2015, Article ID 608325
58. Rocha LCS, Paiva AP, Balestrassi PP, Severino G, Rotela Junior P (2015b) Entropy-based weighting applied to normal boundary intersection approach: the vertical turning of martensitic gray cast iron piston rings case. *Acta Scientiarum Technology* 37(4):361–371
59. Shannon CE (1948) A mathematical theory of communication. *Bell Syst Tech J* 27: 379–423 and 623–656, (July and October)
60. Rocha LCS, Paiva AP, Paiva EJ, Balestrassi PP (2015c) Comparing DEA and principal component analysis in the multiobjective optimization of P-GMAW process. *J Braz Soc Mech Sci Eng, IN PRESS*. DOI 10.1007/s40430-015-0355-z
61. Zahran A, Anderson-Cook CM, Myers RH (2003) Fraction of design space to assess prediction capability of response surface designs. *J Qual Technol* 35(4):377–386